The Sensitivity of Single Polarization Weather Radar Beam Blockage Correction to Variability in the Vertical Refractivity Gradient

JOAN BECH

Catalan Meteorological Service, Barcelona, Spain

BERNAT CODINA AND JERONI LORENTE

Department of Astronomy and Meteorology, University of Barcelona, Barcelona, Spain

DAVID BEBBINGTON

Wave Propagation and Remote Sensing Laboratory, University of Essex, Wivenhoe Park, Colchester, United Kingdom

(Manuscript received 18 August 2002, in final form 21 December 2002)

ABSTRACT

Radars operating in complex orographic areas usually suffer from partial or total beam blockage by surrounding targets at their lowest elevation scans. The need for radar quantitative precipitation estimates in such environments led to the development of beam blockage corrections. This paper aims at evaluating the performance of beam blockage corrections under different electromagnetic propagation conditions with particular interest in anaprop situations. Three years of radiosonde data collected at Barcelona, Spain, a typical Mediterranean coastal site, are used to characterize the behavior of the vertical refractivity gradient near a weather radar. Three different targets surrounding the radar have been chosen and used to evaluate the different beam shielding simulated under different propagation conditions. A simple interception function between the radar beam and the topography is proposed and used for the different targets and propagation conditions considered. Results show that beam blockage correction is generally robust, with departures of 1 dB from the standard propagation conditions correction less than 10% of the time. However, as the presence of extreme anaprop cases would lead to higher differences, the monitoring of the propagation conditions is suggested as a criteria to be considered, among others such as the analysis of the echo structure, as a quality control of the radar quantitative precipitation estimate.

1. Introduction

Weather radars operating in complex orographic areas usually suffer from partial or total beam blockage caused by surrounding mountains. This shielding effect may restrict seriously the use of the lowest antenna elevation angles, which provide the most useful information for rainfall rate estimation at ground level as discussed by Joss and Waldvogel (1990), Sauvageot (1994), Collier (1996), and Smith (1998).

Therefore, in mountainous areas, beam blockage correction schemes may be applied in order to minimize the effect of topography, especially if quantitative precipitation estimations (QPEs) are required. Such corrections are usually included in operational QPE procedures as can be seen in, for example, Harrold et al. (1974), Kitchen et al. (1994), Joss and Lee (1995), Fulton et al. (1998), and Seltmann and Reidl (1999).

Corresponding author address: Joan Bech, Catalan Meteorological Service, Berlin 38, 4. Barcelona 08029, Catalunya, Spain.
E-mail: jbech@meteocat.com

The development of measurement techniques with polarimetric weather radars led to another promising approach to the radar beam blocking problem. Blackman and Illingworth (1995), Zrnic and Ryhzkov (1996), Ryhzkov and Zrnic (1998), and Vivekanandan et al. (1999) showed that, among other advantages, the use of specific propagation phase K_{DP} measurements produce better QPEs under beam blockage conditions than single polarization reflectivity measurements do. However, most operational weather radars still use single polarization systems. For example, in Europe (Meischner et al. 1997) there are some multipolarimetric research radars and only a few operational polarimetric systems though mostly providing differential reflectivity Z_{DR} measurements (cf. Alberoni et al. 2000; Bechini et al. 2002). Therefore, beam blockage corrections of single polarization reflectivity remain a necessary common procedure to provide radar-based QPE in mountainous areas. Because of the usually lower density of surface observing networks and the higher complexity of precipitation patterns in comparison to flat zones, in moun-

tainous areas radar QPE is of particular interest (see, e.g., Westrick et al. 1999; Hagen et al. 2000; Volkert 2000).

The idea that assuming normal propagation conditions for radar observations may not always be a good choice—though it is probably the best option as a first guess—is by no means new and the use of climatological refractive data for a specific radar site was already proposed, for example, in the European Cooperation in the Field of Scientific and Technical Research (COST) 73 Project (Newsome 1992) and, in a different context, evaluated by Pittman (1999) to improve radar height measurements.

In this paper the effect of changing the radar beam propagation conditions upon an ordinary single polarization reflectivity blockage correction is examined. A simplified interception function between the radar beam and topography is proposed to simulate particular results for the Vallirana weather radar, located at 650 m above sea level near Barcelona (northeast Spain) in a complex orography zone, considering real atmospheric propagation conditions. Section 2 describes how average and extreme values of the radar propagation conditions are obtained from a set of radiosonde measurements collected in Barcelona. The interception function between the radar beam and topography is explained in section 3, and in section 4 a discussion of the simulated beam blockage variability and its effects on the shielding correction is provided.

2. Refractivity and anomalous propagation

a. Refractivity gradients

As changes in the bending of the radar beam are due to relatively small variations of the air refractive index n, the magnitude known as refractivity N is commonly used in propagation studies. Bean and Dutton (1968) showed that N can be written as

$$N = (n - 1)10^6 = \frac{77.6}{T}\left(p + \frac{4810e}{T}\right), \qquad (1)$$

where T is the air temperature (K), p is the atmospheric pressure (hPa), and e is the water vapor pressure (hPa). The constants in this equation were determined empirically and are valid for frequencies between 1 and 100 GHz.

The vertical refractivity gradient (VRG), especially in the lowest kilometer above ground level, controls the refraction of the radar beam and, therefore, it is essential for characterizing the radar signal propagation. Moreover, VRG is usually much more important than the horizontal refractivity gradient and, therefore, lateral homogeneity is usually assumed.

A standard atmosphere has associated a vertical refractivity gradient ranging from 0 to -78.7 km^{-1} in the first kilometer above sea level (Skolnik 1980). An increase of VRG (assuming positive values) bends the radar beam more slowly than normal (subrefraction) and reduces the microwave radar horizon. With regard to ground clutter echoes, subrefraction implies a decrease in their frequency and intensity.

On the other hand, a decrease of VRG generates the opposite effect, bending the beam faster than normal (superrefraction) for the interval between -78.7 and -157 km^{-1}. Trapping, or ducting, the most extreme case of anomalous propagation, occurs for values lower than -157 km^{-1}, and in this case the microwave energy may travel for long distances before intercepting ground targets producing anomalous propagation (i.e., anaprop or AP) echoes. In fact, a careful analysis of the fluctuation of target reflectivity may be a way to monitor variations in atmospheric conditions, as shown by Fabry et al. (1997).

Superrefraction, and ducting in particular, is usually associated with temperature inversions or sharp water vapor gradients. During cloudless nights, radiation cooling over land favors the formation of ducts, which disappear as soon as the sun heats the soil surface destroying the temperature inversion. Sometimes this process may be clearly observed in the daily evolution of clutter echoes, as reported by Moszkowicz et al. (1994) and others.

b. Radiosonde data and VRG calculations

As radiosoundings have been traditionally the only source of upper-air information available on a routine basis, they have been used for years to calculate long-term averages of propagation conditions; see, for example, Gossard (1977) or Low and Hudak (1997).

In this study, propagation conditions have been calculated from 1200 UTC (1200 LST) radiosonde observations collected in Barcelona using Vaisala RS-80 sondes between 1997 and 2000 [see Bech et al. (2000) for more details]. The sondes sampled every 10 s provided much higher vertical resolution than the usual standard operational radiosounding observations. This allowed better characterization of the air refractive index variability and the detection of thinner superrefractive layers that may not be detected by standard radiosounding observations but may have significant effects in the propagation of the radar beam.

After quality controlling the data, 862 radiosoundings representing all seasons were selected. This dataset may be considered a good representation of climatology and provides enough variety to produce different results in the radar beam blockage corrections analysis. The data were used to calculate duct occurrence and vertical refractivity gradients for individual layers contained in the first 1000 m above ground level and also to determine the average gradient for the whole layer of 1 km above ground level. This average gradient was determined as the variation of refractivity from the bottom to the top of the layer, following the recommendations

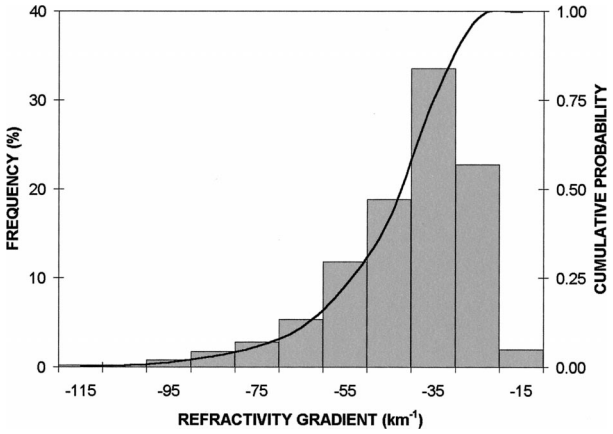

FIG. 1. Frequency histogram and cumulative probability plot of the vertical refractivity gradient in the first 1000 m AGL for 1200 UTC Barcelona radiosonde measurements.

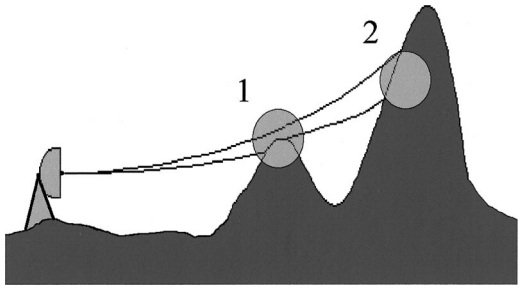

FIG. 2. Example of partial "1" and total "2" beam blockage of a radar operating in complex topography. The measurements of the beam region between 1 and 2 may be modified by a beam blockage correction.

of the International Telecommunication Union (ITU 1997).

The Barcelona 1200 UTC VRG measurements were grouped in 21 equally spaced classes of 5-km^{-1} intervals, ranging from -115 to -15 km^{-1}. Figure 1 shows the cumulative frequency distribution and the histogram of the vertical refractivity gradient classes for Barcelona in the first 1000 m above ground level.

The mode value of the VRG for the first 1000 m was -40 km^{-1} (standard propagation), the maxima and minima were -119 and -15 km^{-1}, respectively, and 2% of the cases presented VRG below -90 km^{-1}. Regarding the presence of thinner superrefractive layers within the first 1000 m, ducts appeared in 37% of all individual layers analyzed and 60% of them had refractive gradients below 300 km^{-1}.

An analysis of a larger radiosonde dataset recorded in Barcelona containing also 0000 UTC (local midnight) observations (Bech et al. 2002), confirms that VRG at 1200 UTC shows, as expected, less superrefraction than those recorded at 0000 UTC. This is due, most probably, to the dominant effect of nocturnal radiative cooling, which results in low-level inversion.

This larger dataset was made up of 2140 radiosoundings (864 corresponding to 1200 UTC and 1276 to 0000 UTC). From this dataset, the difference of median values of VRG between 0000 and 1200 UTC was used to estimate the VRG diurnal range. On average, a difference of 7 N units km^{-1} was found between midday and midnight measurements. However, this daily range varies widely throughout the year: in summer months it may reach more than double (18 N units km^{-1} in August), and in winter the range is reduced to 1 or 2 N units km^{-1}.

3. Radar beam blockage

a. Interception function

To describe in full detail the interception of the energy transmitted by the radar with the surrounding topography, a precise description of the antenna radiation pattern would be required. As this pattern is rather complex, it is common to assume the usual geometric-optics approach and consider that the radar energy is concentrated in the main lobe of the radar antenna pattern (Skolnik 1980). Then, when a radar beam intercepts a mountain, two situations are possible (Fig. 2): 1) only part of the beam cross section illuminates the intercepted topography (partial blockage), or 2) the radar beam is completely blocked (total blockage).

The percentage area of the radar beam cross section blocked by topography may be expressed as a function of the radius of the beam cross section a and the difference of the average height of the terrain and the center of the radar beam y (see Fig. 3). Depending on the relative position of the beam height respect to topography, y may be either positive or negative.

According to these definitions, partial beam blockage occurs when $-a < y < a$, total beam blockage means that $y \geq a$ and, finally, $y \leq -a$ implies there is no blockage at all. Using the notation introduced above, it can be seen that partial beam blockage (PBB) may be written as (see the appendix for more details)

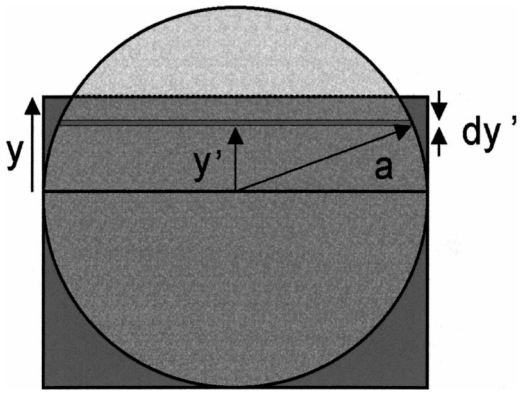

FIG. 3. Elements considered in the radar beam blockage function: a is the radius of the radar beam cross section, y the difference between the center of the radar beam and the topography, dy' the differential part of blocked beam section, and y' the distance from the center to dy'.

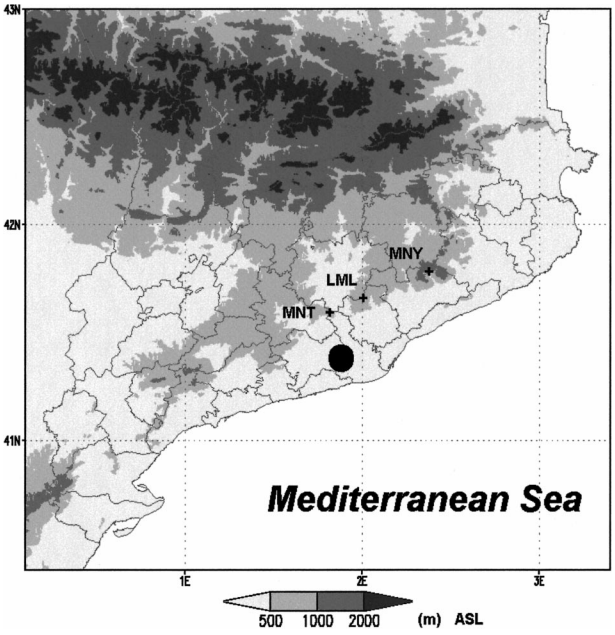

FIG. 4. Topographical map of Catalonia showing the geographical distribution of ground targets (crosses) around the Vallirana radar (circle).

$$\mathrm{PBB} = \frac{y\sqrt{a^2 - y^2} + a^2 \arcsin\frac{y}{a} + \frac{\pi a^2}{2}}{\pi a^2}. \quad (2)$$

On the other hand, the height of the center of the radar beam h is given at a distance r by the expression (see, e.g., Doviak and Zrnic 1993)

$$h = \sqrt{r^2 + (k_e R)^2 + 2rk_e R \sin\theta} - k_e R + H_0, \quad (3)$$

where R is the earth's radius, k_e is the ratio between R and the equivalent earth's radius, θ is the antenna elevation angle, and H_0 is the antenna height.

Information about atmospheric propagation conditions is contained in k_e, which may be written in terms of the refractivity gradient as

$$k_e = \frac{1}{1 + R\left(\frac{dN}{dh}\right)}. \quad (4)$$

The usual value for k_e in the first kilometer of the troposphere, assuming the normal VRG of -40 km^{-1}, is approximately 4/3.

Substituting (4) and (3) in (2), an expression of the beam blockage in terms of the propagation conditions is obtained (further details may be found in the appendix).

b. Ground targets

When the first clutter maps for the Spanish weather service Instituto Nacional de Meteorología (INM) radar network were built, the combination of complex orography and coastal anaprop prone zones was already identified as a factor that increased blocked areas (Camacho and Lamela 1996) as may happen elsewhere when these conditions are met. The topography of Catalonia, located in the northeast of the Iberian Peninsula, is made up of a number of mountain ranges distributed in different orientations. The Pyrenees dominate the northern sector with heights up to 3000 m above sea level, while parallel to the coast there are some massifs conforming the coastal and precoastal ranges with maximum altitudes around 1000 and 1700 m.

TABLE 1. Distance to the radar and height of selected ground clutter targets.

Target	Distance (km)	Height (m)
MNT	26	1100
LML	32	1000
MNY	65	1400

Three clutter targets that presented partial beam blockage under normal propagation conditions were chosen to examine the effects of changing the VRG. Figure 4 shows a topographic map of Catalonia and indicates the location of the selected targets and the Vallirana radar (41°22′28″N, 1°52′52″E). The Vallirana radar is a C-band Doppler system with a 1.3° beamwidth antenna at 3 dB. The targets chosen are normally used to check the radar antenna alignment on a routine basis and are located within the region of interest of radar QPE. Table 1 gives some details of each target, namely, the distance to the radar and the average height intercepted by the radar beam obtained from a digital elevation model. The targets were located at different ranges, had different heights, and showed different degrees of blockage, in order to be representative of the topography surrounding the radar. They are located in the so-called precoastal range sharing a similar propagation environment and comparable to that obtained by the Barcelona radiosonde. For example, the area considered is usually influenced by a marked sea-breeze circulation pattern, just like the city of Barcelona (Redaño et al. 1991).

c. Beam blocking correction

To evaluate the effects of anomalous propagation, the partial beam blocking correction scheme used in the Next Generation Weather Radar (NEXRAD) Precipitation Processing System has been considered. This scheme (Fulton et al. 1998) is applied to radar beams partially shielded (see Table 2).

In particular, this type of beam blockage correction is applied to radar pixels (or radar bins) whose shielding ranges between 10% and 60%, and it consists of modifying radar equivalent reflectivity factor measurements

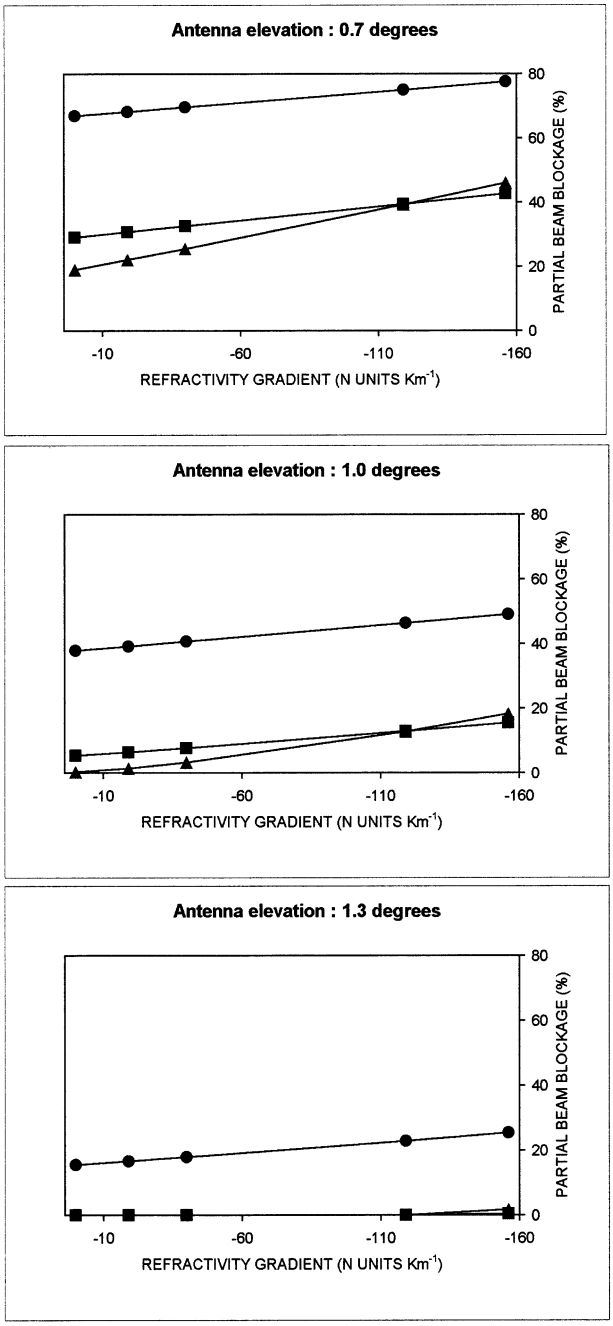

FIG. 5. Simulated partial beam blockage vs refractivity gradient plot for three selected clutter targets (MNT, circle; LML, square; and MNY, triangle) at three antenna elevations: 0.7°, 1.0°, and 1.3°.

by adding 1–4 dB depending on the degree of occultation. The correction is also applied to all pixels further out in range of the same blocked radar ray, neglecting diffraction below the shadow boundary.

The correction depends only on the percentage of beam cross section shielded and, in the description provided by Fulton et al. (1998), no specific mention is made about which part of the beam is shielded. This approach allows consideration of a simple interception function, as the one proposed in the previous section, assuming that the correction additive factors contain considerations about interception details such as the beam power distribution.

This beam blockage procedure is used with other corrections such as a test on the vertical echo continuity and a sectorized hybrid scan (Shedd et al. 1991). Other approaches to this question with different degrees of sophistication have been used in the past (see, e.g., Delrieu et al. 1995; Gabella and Perona 1998; Michelson et al. 2000). All of them have in common the assumption of standard propagation conditions of the radar beam.

4. Results and discussion

a. Refractivity gradient versus beam blockage

The radar beam blockage under a particular VRG can be simulated considering both the observed propagation conditions and the interception function described in the previous sections. This may be achieved by assuming an homogeneous VRG for the whole radar beam and calculating the associated beam blockage for each selected target for a given initial antenna elevation angle.

In Fig. 5 a set of beam blockages versus VRG plots is shown for different antenna elevation angles. The refractivity gradient values considered contain the observed extreme VRG values (-119 and -15 km^{-1}) and are also extended to include pure subrefraction (0 km^{-1}) and almost ducting conditions (-156 km^{-1}) to illustrate their effects. These extreme cases seem realistic taking into account the presence of thin ducting layers, as mentioned in section 2, that may have high VRGs embedded in others with lower VRGs, considering the fact that the bending of the ray path is an additive process throughout the whole layer crossed by the radar beam.

As expected, as the antenna angle increases, beam blockage is reduced. For example, for an antenna elevation of 0.7° a relatively high beam blockage rate is expected, as the lowest part of the main lobe in a 1.3° beamwidth antenna is pointing to the surrounding hills, producing values of blockage ranging mostly between 30% and 80%. On the other hand, the 1.3° elevation beam blockage values are mostly below 20% and for some targets are always null (no blockage at all) except for the most superrefractive situations. The 1° elevation beam represents an intermediate situation that lies between the last two cases.

Depending on the particular geometry of the beam interception of each target, the rate of increase of blocking with the variation of the vertical refractivity gradient may be different. In the cases shown, the farthest target, MNY, exhibits a larger blockage for very superrefractive situations than LML, unlike in normal and subrefractive conditions.

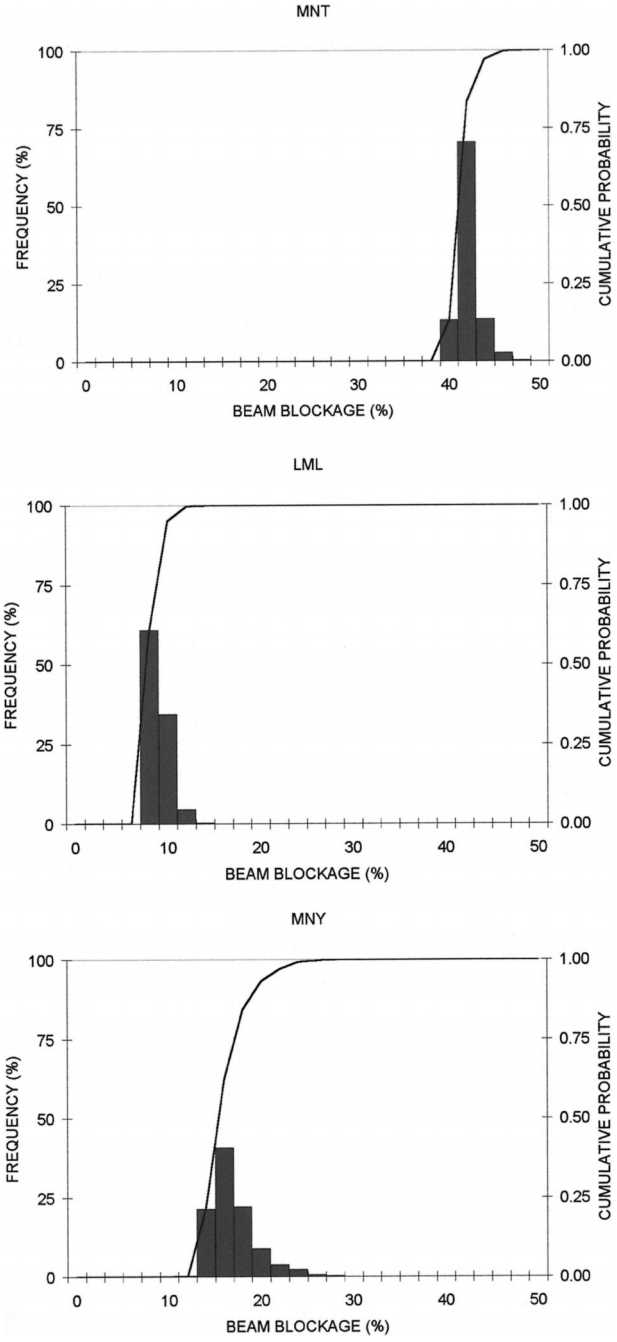

FIG. 6. Frequency histograms and cumulative distributions for radar beam blockage considering interceptions of an initial antenna elevation angle of 1° with three different ground targets: MNT, LML, and MNY.

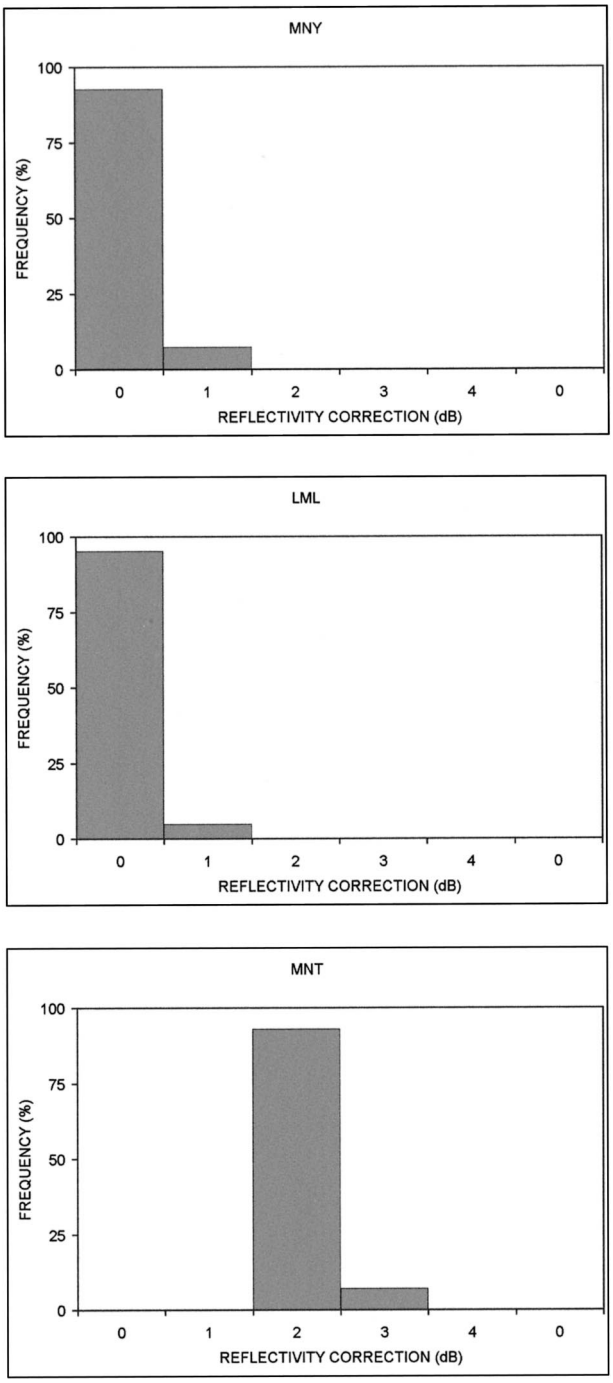

FIG. 7. Frequency histograms of beam blockage corrections considering interceptions of an initial antenna elevation angle of 1° with three different ground targets: MNT, LML, and MNY.

b. Beam blockage variability

Considering the frequency distribution of VRG previously shown, an assessment on the corresponding beam blockage variability may be made for a particular target. In this case, only real VRG data observed are considered so no extreme values are added to extend the VRG range as before. In principle, this should produce a more conservative, or smoothed, result; yet, as discussed in section 2, it seems more realistic to consider that more superrefraction than reflected by the VRG histogram cases takes place in reality.

Figure 6 shows histograms of beam blockage fre-

TABLE 2. Partial occultation corrections (after Fulton et al. 1998).

Occultation (%)	Reflectivity correction (dB)
0–10, >60	0
11–29	+1
30–43	+2
44–55	+3
56–60	+4

TABLE 3. Partial occultation corrections for three targets with different propagation conditions for antenna elevation of 1°.

	Vertical refractivity gradient (N units km^{-1})				
	0	−19	−40	−119	−156
Target	Reflectivity correction (dB)				
MNT	2	2	2	3	3
LML	0	0	0	1	1
MNY	0	1	1	1	1

quency and the corresponding cumulative probability for a number of selected targets intercepted by a 1° elevation radar beam. These histograms have been derived considering beam blockage classes of 2%. The nearest targets, namely, MNT and LML, show a moderate (around 40%) to low (10%) rate of beam blockage, respectively. The most distant target, MNY, intercepts the radar beam mostly between 8% and 14%. The range of variations in the beam blockage observed in the above-mentioned histograms oscillates from 8% (LML) and 10% (MNT) to 18% (MNY). From the cumulative probability plots it may be noted that both MNT and LML show single classes representing more than 50% while a more smoothed distribution is found for MNY.

Considering the beam blockage correction described in section 3, a frequency histogram of the beam blockage correction may be built for a given target. This is shown in Fig. 7 where the histogram of the reflectivity correction given in Table 2 is depicted for each target and beam blockage distribution shown in Fig. 6.

Should the beam blockage correction have been a continuous function, where for a particular value of blockage a different correction factor would be applied, then the spread of the beam blockage histograms would have been reflected in the spread of the correction histograms. However, this is not the case for the particular type of correction considered where only four different correction values are possible depending on the beam blockage. Therefore, a big variability in the beam blockage occurrence does not necessarily produce the same variability in the blockage correction.

This effect is illustrated by the distant target MNY where a relatively high variability in the blockage (10%–16%) does produce only two possible different correction values, just like the other targets with less variability. The change from one correction factor to the other is produced always under superrefractive conditions, so in this case, subrefraction is not relevant enough to produce significant changes in the beam, as might be anticipated from the VRG histogram, which shows a much shorter tail in the subrefractive area than in the super refractive one.

Despite the variance shown in the blockage correction, it is important to note that, in the three cases considered, the most usual blockage correction occurs more than 85% of the time, so, in principle, the beam blockage correction may be considered reasonably robust. However, the occurrence of intense ducts shown by the radiosonde data analysis indicates that greater differences in corrections values than those shown in Table 3 are possible. Though it is difficult to quantify the frequency at which these extreme VRGs do occur, as discussed before, the effects of embedded ducting layers in apparently more smoothed VRGs should be cautiously considered.

c. VRG diurnal range

As seen in section 2, the yearly averaged diurnal range of VRG is, approximately, 7 N units km^{-1} and in summer is increased to 18 N units km^{-1}. From the point of view of the radar beam blockage, this range implies quite a limited effect as may be noted in Fig. 8. It shows a simulation of the beam blockage for an antenna elevation angle of 1° and also plots the simulated blockage considering two possible diurnal ranges (7 and 18 N units km^{-1}). The differences in the blockage are between 1% and 2% so, in general, they do not have significant effects in the corrections. Another remark about the average VRG diurnal range is that, given its relatively low value, changes in the VRG usually happen at a larger scale than a single day and, therefore, are more noticeable on a month-to-month basis.

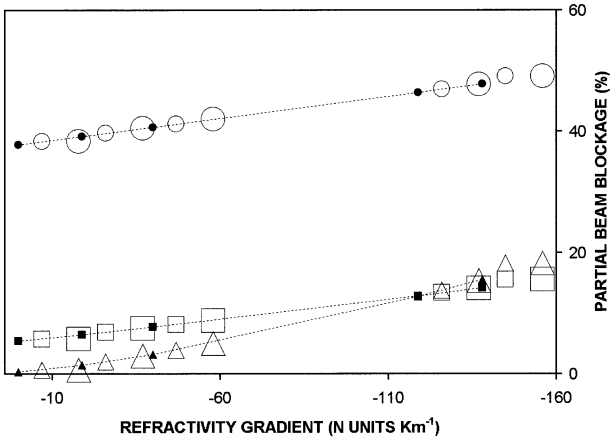

FIG. 8. Simulation of the differential blockage produced by the diurnal range of VRG: small solid symbols correspond to 1200 UTC and medium and bigger symbols to 0000 UTC for an average and summer diurnal range, respectively. The three ground targets considered are MNT (circle), LML (square), and MNY (triangle).

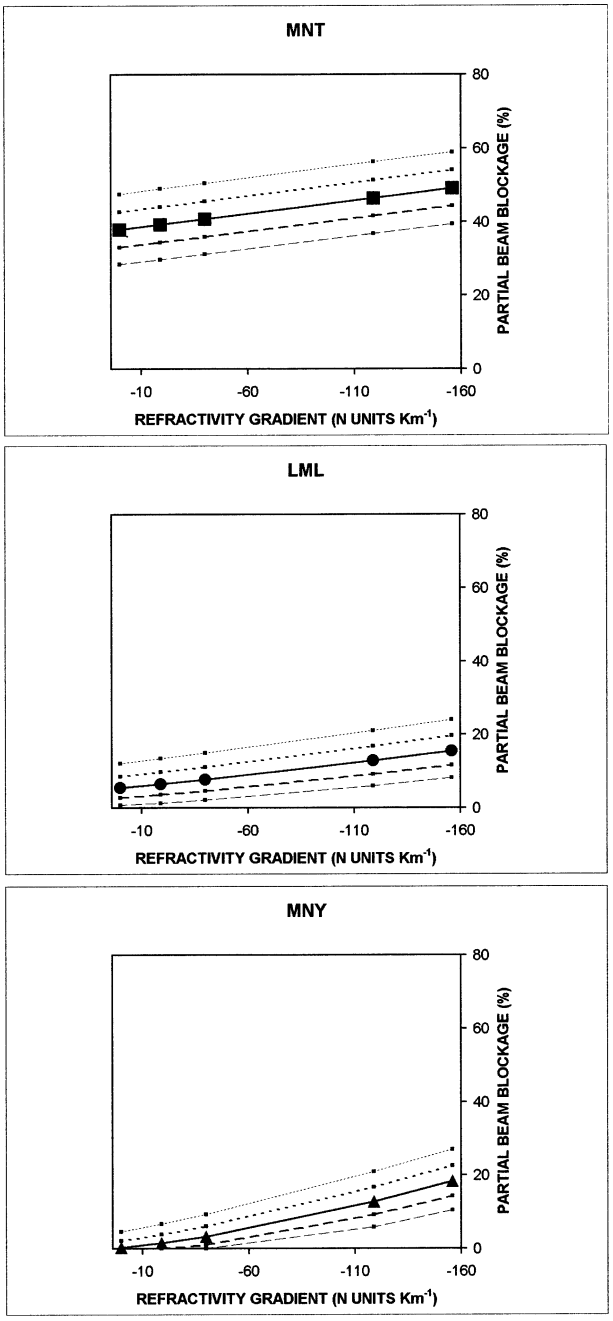

FIG. 9. Simulated beam blockage for an antenna elevation of 1° and the values corresponding to standard errors in the antenna pointing accuracy of 0.10° and 0.05° evaluated at targets MNT, LML, and MNY.

d. Antenna pointing accuracy

Another source of variability in the occultation corrections is the pointing accuracy of the antenna. The relative importance of this effect is displayed in Fig. 9. It shows a simulation of the radar beam blockage produced with an antenna elevation of 1° at the three selected targets compared with the different blockage caused by mean standard errors of 0.10° and 0.05° in the antenna elevation.

The 0.10° errors are very relevant and produce significant effects, comparable or even larger than those attributed to the variability of the VRG (around 10% in the beam blockage). The 0.05° pointing errors induce shielding variations of 5% in the beam blockage, more than twice the variation caused by an average VRG summer daily range.

5. Conclusions

In this paper radiosonde measurements are used to model radar propagation trough the lower atmosphere and to assess the variability of beam blockage corrections. A histogram of occultation corrections for several ground targets is performed using a simple beam-geometric approach and a sounding-based climatology of vertical gradients of the refractive index.

The analysis performed shows that under anaprop conditions, partial beam blockage corrections based on assuming standard propagation may lead to inaccurate results, comparable, in extreme cases, to those derived from a poorly calibrated antenna alignment. As shown in previous sections, the variability of the correction is generally small and, in moderately intense superrefractive situations, exceeds 1 dB with respect to the correction under standard propagation conditions. However, severe superrefractive cases may cause bigger differences. For instance, extreme anaprop cases where partial beam blockage is incremented significantly but does not reach 60% and is not detected in a vertical echo continuity test may produce a wrong correction of 2 or even 3 dB in the beam blockage correction scheme discussed here. Such errors may be significant, especially if the propagation conditions persist over a long period of time and, obviously, if they occur at the same time that precipitation takes place. The potential errors derived from wrong beam blockage corrections in extreme anaprop cases may be more important than the usual limitations of operational radar hardware calibration and stability.

To detect such cases, information about the observed or forecasted VRG in the radar coverage area, if available, might be incorporated in the correction schemes as a quality control. Apart from anaprop echoes caused by small-scale features such as thunderstorm outflows (Weber et al. 1993), information about VRG could provide a good general overview of the radar propagation conditions over a larger timescale and spatial scale and, therefore, about the degree of adequacy of the beam blockage corrections performed.

Hence, taking into account the results exposed above, in locations where radar QPE require beam blockage corrections, it seems reasonable to examine the VRG of the area to check its variability and its potential influence on the blockage correction. Moreover, from an opera-

tional perspective, if it is feasible to have an estimation of the VRG in the radar coverage area, either from radiosonde observations or from mesoscale NWP output as described by Johnson et al. (1999), then it may be incorporated among other criteria, such as a three-dimensional analysis of the radar echo structure (Krajewski and Vignal 2001; Steiner and Smith 2002), to improve the identification of AP in radar images as a quality control of the QPE procedure.

Acknowledgments. The work reported in this paper was funded by the EU project CARPE-DIEM (Critical Assessment of available Radar Precipitation Estimation techniques and Development of Innovative approaches for Environmental Management, Contract EVG1-2001-00031) and was done within the framework of the EU COST-717 action ''Use of weather radar observations in numerical weather prediction and hydrological models.'' We gratefully appreciate the enthusiastic support offered by Tage Anderson from the Swedish Meteorological and Hydrological Institute at the early stage of the work and also useful comments about beam blockage experienced by several Spanish weather radars kindly provided by José Luis Camacho from the Instituto Nacional de Meteorología. Authors also appreciate deeply two anonymous reviewers whose constructive comments helped to improve the final form of this paper.

APPENDIX

A Simplified Beam Interception Function

A simplified interception function between the radar beam cross section and the topography may be deduced in order to calculate the beam blockage (BB). According to Fig. 3, given a circle of radius a, and a height difference of the center of the radar beam with respect to topography y, a differential part of the radar beam, dBB, is given by

$$d\mathrm{BB} = dy' 2\sqrt{a^2 - y'^2}, \tag{A1}$$

where y' is the height from the center of the circle and dy the thickness of the shaded area.

Integrating (A1) from the bottom of the radar beam cross section to the height given by y', then the beam blockage is

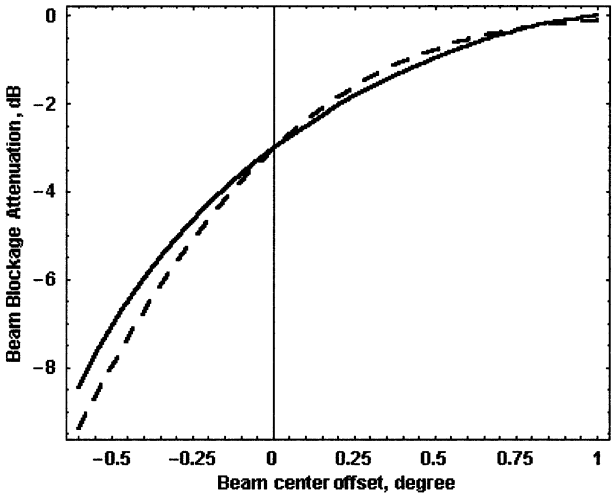

FIG. A1. Comparison of the effect of equivalent beam blockage on a uniform beam (dashed line) and a Gaussian beam (solid line) each of 1.3° half-power full beamwidth.

$$\begin{aligned}\mathrm{BB} &= \int_{-a}^{y} 2\sqrt{a^2 - y'^2}\, dy' \\ &= 2\left[\frac{y'^2}{2}\sqrt{a^2 - y'^2} + \frac{a^2}{2}\arcsin\frac{y'}{a}\right]_{-a}^{y} \\ &= y\sqrt{a^2 - y^2} + a^2 \arcsin\frac{y}{a} + \frac{\pi a^2}{2}. \end{aligned} \tag{A2}$$

PBB may be considered as the ratio between BB and the whole radar cross section (i.e., the circle of radius a). Then, from Eq. (A2), partial beam blockage may be written simply as

$$\begin{aligned}\mathrm{PBB} &= \frac{y\sqrt{a^2 - y^2} + a^2 \arcsin\frac{y}{a} + \frac{\pi a^2}{2}}{\pi a^2} \\ &= \frac{1}{\pi}\left[\frac{y}{a^2}\sqrt{a^2 - y^2} + \arcsin\left(\frac{y}{a}\right) + \frac{\pi}{2}\right]. \end{aligned} \tag{A3}$$

Considering an antenna main lobe beam width given by the angle β, at a given distance r from the radar, then the radius a of the beam cross section is

$$a = \frac{r\beta}{2}. \tag{A4}$$

Substituting Eqs. (3), (4), and (A4) in (A3), an expression of PBB relating the propagation conditions may be written as

$$\mathrm{PBB} = \frac{1}{\pi}\left\{\frac{4(z + k_e R - \sqrt{r^2 + k_e^2 R^2 + 2rk_e R\sin\theta} - H_a)}{r^2\beta^2}\sqrt{\frac{r^2\beta^2}{4} - (z + k_e R - \sqrt{r^2 + k_e^2 R^2 + 2rk_e R\sin\theta} - H_0)^2}\right.$$
$$\left. + \arcsin\left[\frac{2(z + k_e R - \sqrt{r^2 + k_e^2 R^2 + 2rk_e R\sin\theta} - H_0)}{r\beta}\right] + \frac{\pi}{2}\right\}.$$

The exact effects of beam blockage will, in general, depend on the shape of the beam profile. An idealized profile as adopted here enables the ''practical'' cases of either no blocking or complete blocking to be identified by simple criteria. Slightly less idealized, but more realistic, is the case of a Gaussian beam. A comparison between two equivalent beams is shown in Fig. A1. The differences between the two show up only at the extremes and on a logarithmic scale only become significant where the loss due to blockage is several decibels, which is beyond the limit of applicability of the considered corrections.

REFERENCES

Alberoni, P. P., V. Levizzani, R. J. Watson, A. R. Holt, S. Costa, P. Mezzasalma, and S. Nanni, 2000: The 18 June 1997 companion supercells: Multiparametric Doppler radar analysis. *Meteor. Atmos. Phys.,* **75,** 101–120.

Bean, B. R., and E. J. Dutton, 1968: *Radio Meteorology*. Dover, 435 pp.

Bech, J., A. Sairouni, B. Codina, J. Lorente, and D. Bebbington, 2000: Weather radar anaprop conditions at a Mediterranean coastal site. *Phys. Chem. Earth (B),* **25,** 829–832.

——, B. Codina, J. Lorente, and D. Bebbington, 2002: Monthly and daily variations of radar anomalous propagation conditions: How ''normal'' is normal propagation? *Proc. Second European Meteorological Radar Conf.,* Delft, Netherlands, Copernicus GmbH, 35–39.

Bechini, R., E. Gorgucci, G. Scarchilli, and S. Dietrich, 2002: The operational weather radar of Fossalon di Grado (Gorizia, Italy): Accuracy of reflectivity and differential reflectivity measurements. *Meteor. Atmos. Phys.,* **79,** 275–284.

Blackman, T. M., and A. J. Illingworth, 1995: Improved measurements of rainfall using differential phase techniques. *COST 75 Int. Seminar on Weather Radar Systems,* Brussels, Belgium, European Commission, EUR 16013 EN, 662–671.

Camacho, J. L., and P. Lamela, 1996: Mapping blocked and blind areas in the Spanish INM radars. COST 75 Working Document, 11 pp. [Available from Instituto Nacional de Meterología (INM), Apartado 285, 08080 Madrid, Spain.]

Collier, C. G., 1996: *Applications of Weather Radar Systems.* Wiley, 390 pp.

Delrieu, G., J. D. Creutin, and H. Andrieu, 1995: Simulation of radar mountain returns using a digitized terrain model. *J. Atmos. Oceanic Technol.,* **12,** 1038–1049.

Doviak, R. J., and D. S. Zrnic, 1993: *Doppler Radar and Weather Observations.* Academic Press, 562 pp.

Fabry, F., C. Frush, I. Zawadki, and A. Kilambi, 1997: On the extraction of near-surface index of refraction using radar phase measurements from ground targets. *J. Atmos. Oceanic Technol.,* **14,** 978–987.

Fulton, R. A., J. P. Breidenbach, D. Seo, D. Miller, and T. O'Bannon, 1998: The WSR-88D rainfall algorithm. *Wea. Forecasting,* **13,** 377–395.

Gabella, M., and G. Perona, 1998: Simulation of the orographic influence on weather radar using a geometric-optics approach. *J. Atmos. Oceanic Technol.,* **15,** 1486–1495.

Gossard, E. E., 1977: Refractive index variance and its height distribution in different air masses. *Radio Sci.,* **12,** 89–105.

Hagen, M., H. H. Schiesser, and M. Dorninger, 2000: Monitoring of mesoscale precipitation systems in the Alps and the Northern Alpine Foreland by radar and rain gauges. *Meteor. Atmos. Phys.,* **72,** 87–100.

Harrold, T., E. English, and C. Nicholass, 1974: The accuracy of radar-derived rainfall measurements in hilly terrain. *Quart. J. Roy. Meteor. Soc.,* **100,** 201–208.

ITU, 1997: The radio refractive index: Its formula and refractivity data. ITU-R P-Series, Doc. ITU-R P.453-6, ITU Radiocommunication Assembly, 9 pp.

Johnson, C., D. Harrison, and B. Golding, 1999: Use of atmospheric profile information in the identification of anaprop in weather radar images. Observations Based Products Tech. Rep. 17, Meteorological Office, Bracknell, United Kingdom, 30 pp.

Joss, J., and A. Waldvogel, 1990: Precipitation measurement and hydrology, A review. *Radar in Meteorology,* D. Atlas, Ed., Amer. Meteor. Soc., 577–606.

——, and R. Lee, 1995: The application of radar–gauge comparisons to operational precipitation profile corrections. *J. Appl. Meteor.,* **34,** 2612–2630.

Kitchen, M., R. Brown, and A. G. Davies, 1994: Real-time correction of weather radar data for the effects of bright band, range and orographic growth in widespread precipitation. *Quart. J. Roy. Meteor. Soc.,* **120,** 1231–1254.

Krajewski, W. F., and B. Vignal, 2001: Evaluation of anomalous propagation echo detection in WSR-88D data: A large sample case study. *J. Atmos. Oceanic Technol.,* **18,** 807–814.

Low, T. B., and D. R. Hudak, 1997: Development of air mass climatology analysis for the determination of characteristic marine atmospheres. Part I: North Atlantic. *Theor. Appl. Climatol.,* **57,** 135–153.

Meischner, P., C. G. Collier, A. Illingwoth, J. Joss, and W. Randeau, 1997: Advanced weather radar systems in Europe: The COST 75 action. *Bull. Amer. Meteor. Soc.,* **78,** 1411–1428.

Michelson, D. B., and Coauthors, 2000: BALTEX radar data centre products and their methodologies. RMK 90, Swedish Meteorological and Hydrological Institute, Norrköpping, Sweden, 76 pp.

Moszkowicz, S., G. J. Ciach, and W. F. Krajewski, 1994: Statistical detection of anomalous propagation in radar reflectivity patterns. *J. Atmos. Oceanic Technol.,* **11,** 1026–1034.

Newsome, D. H., 1992: Weather Radar Networking COST Project 73 Final Report. Kluwer Academic, 254 pp.

Pittman, T. S., 1999: A climatology-based model for long-term prediction of radar beam refraction. M.S. thesis, U.S. Air Force Institute of Technology, 184 pp.

Redaño, A., J. Cruz, and J. Lorente, 1991: Main features of sea breeze in Barcelona. *Meteor. Atmos. Phys.,* **46,** 175–179.

Ryhzkov, A. V., and D. S. Zrnic, 1998: Polarimetric rainfall estimation in the presence of anomalous propagation. *J. Atmos. Oceanic Technol.,* **15,** 1320–1330.

Sauvageot, H., 1994: Rainfall measurement by radar: A review. *Atmos. Res.,* **35,** 27–54.

Seltmann, J. E. E., and J. Reidl, 1999: Improved clutter treatment within the German radar network: First results. *Proc. COST 75 Int. Seminar on Advanced Weather Radar Systems,* Locarno, Switzerland, European Commission, EUR 18567 EN 267–279.

Shedd, R., J. Smith, and M. Walton, 1991: Sectorized hybrid scan strategy of the NEXRAD precipitation-processing system. *Hydrological Applications of Weather Radar,* I. Cluckie and C. Collier, Eds., Ellis Horwood Limited, 151–159.

Skolnik, M., 1980: *Introduction to Radar Systems.* McGraw-Hill, 581 pp.

Smith, P. L., Jr., 1998: On the minimum useful elevation angle for weather surveillance radar scans. *J. Atmos. Oceanic Technol.,* **15,** 841–843.

Steiner, M., and J. A. Smith, 2002: Use of three-dimensional reflectivity structure for automated detection and removal of nonprecipitating echoes in radar data. *J. Atmos. Oceanic Technol.,* **19,** 673–686.

Vivekanandan, J., D. N. Yates, and E. Brandes, 1999: The influence of terrain on rainfall estimates from radar reflectivity and specific propagation phase observations. *J. Atmos. Oceanic Technol.,* **16,** 837–845.

Volkert, H., 2000: Heavy precipitation in the alpine region (HERA): Areal rainfall determination for flood warnings through in-site

measurements, remote sensing and atmospheric modeling. *Meteor. Atmos. Phys.*, **72,** 73–85.

Weber, M. E., M. L. Stone, and J. A. Cullen, 1993: Anomalous propagation associated with thunderstorm outflows. Preprints, *26th Int. Conf. on Radar Meteorology*, Norman, OK, Amer. Meteor. Soc., 238–240.

Westrick, K., C. Mass, and B. Colle, 1999: The limitations of the WSR88-D radar network for quantitative precipitation measurement over the coastal western United States. *Bull. Amer. Meteor. Soc.,* **80,** 2289–2298.

Zrnic, D., and A. Ryhkov, 1996: Advantages of rain measurements using specific differential phase. *J. Atmos. Oceanic Technol.,* **13,** 454–464.